

# Nanoindentation and nanostructural characterization of ZrB<sub>2</sub>-SiC composite doped with graphite nano-flakes

Mehdi Shahedi Asl<sup>a,\*</sup>, Behzad Nayebi<sup>b</sup>, Amir Motallebzadeh<sup>c</sup>,  
Mohammadreza Shokouhimehr<sup>d,\*\*</sup>

<sup>a</sup> Department of Mechanical Engineering, University of Mohaghegh Ardabili, Ardabil, Iran

<sup>b</sup> Department of Mining and Metallurgical Engineering, Amirkabir University of Technology (Tehran Polytechnic), P. O. Box 15875-4413, Tehran, Iran

<sup>c</sup> Koç University Surface Science and Technology Center (KUYTAM), Sariyer, Istanbul, 34450, Turkey

<sup>d</sup> Department of Materials Science and Engineering, Research Institute of Advanced Materials, Seoul National University, Seoul, 08826, Republic of Korea

## ARTICLE INFO

### Keywords:

Ultrahigh temperature ceramics  
In-situ formed phases  
Spark plasma sintering  
Nanoindentation  
Interfacial characterization  
Electron microscopy

## ABSTRACT

Nano-sized graphite was used as a dopant for fabrication of ZrB<sub>2</sub>-SiC ceramic via spark plasma sintering at 1800 °C for 8 min under 35 MPa. As-sintered composite was characterized by XRD, SEM, EDS, STEM, TEM and nanoindentation in order to study the micro/nanostructure and mechanical properties of the sample. A near fully-dense ternary composite was obtained after densification process. In-situ formation of ZrC was attributed to the chemical reaction of graphite nano-flakes with ZrO<sub>2</sub> nano-layers covered the surface of starting ZrB<sub>2</sub> powders. Reactive role of graphite as an effective sintering aid, via removal of oxide impurities, was illustrated by TEM, as some ultrafine porosities were remained in the sintered bulk in graphite-free areas. The hardness and elastic modulus of the composite, obtained by the nanoindentation method, showed an excellent harmony with the reported data in the literature. The average hardness of 15.2, 18.3 and 10.7 GPa were achieved for ZrB<sub>2</sub>, SiC and ZrB<sub>2</sub>/SiC interface, respectively. Average Young's moduli of matrix and reinforcement phases were measured as 328 and 306 GPa, respectively, which showed favorable adaption in mechanical properties of composite components. The nano-indentational characteristics of composite, especially pop-ins in the load-displacement curves, were also discussed.

## 1. Introduction

Ultrahigh temperature ceramic matrix composites (UHTCMC) comprising binary ZrB<sub>2</sub>-SiC [1–6] and ternary ZrB<sub>2</sub>-SiC-C [7] have an exceptional combination of characteristics such as high electrical and thermal conductivity, superior fracture toughness and bending strength as well as good thermal shock resistance. Previous research works have proved the positive effects of SiC and carbonaceous materials such as carbon black [8,9], carbon fiber [10,11], carbon nanotube [12], graphene [13,14] and graphite [15,16] on densification and thermo-mechanical properties of ZrB<sub>2</sub>-based ceramic matrix composites.

Nevertheless several brilliant reports [17,18] on successful machining of ZrB<sub>2</sub>-SiC composites to obtain near-net shape products, achieving complex geometry components made of such UHTC materials still evokes further investigations, mainly from economical point of view. Promising developments in UHTC manufacturing techniques have

been recently published, which are focused on innovative reinforcing of the materials via combining new synthesis and sintering routes [19].

Spark plasma sintering (SPS) route is a modern densification methodology for manufacturing through powder metallurgy approach [20–24]. In the SPS process, the energy needed for the consolidation of powder particles is supplied by an electrical field. Herein, similar to the hot pressing route, an external load has to be applied on the powder compact during the densification process. Anyway, SPS requires lower sintering temperatures and soaking times in comparison to the conventional methods. Such a newly-developed sintering route has been successfully used for fabrication of UHTCs and their composites [24–31].

To the best of our understanding, there is no comprehensive report on the characterization of spark plasma sintered nano-graphite doped ZrB<sub>2</sub>-SiC ceramics, particularly, using the transmission electron microscopy and nanoindentation methods. Therefore, a nano-scale approach

\* Corresponding author.

\*\* Corresponding author.

E-mail addresses: [shahedi@uma.ac.ir](mailto:shahedi@uma.ac.ir) (M. Shahedi Asl), [mrsh2@snu.ac.kr](mailto:mrsh2@snu.ac.kr) (M. Shokouhimehr).

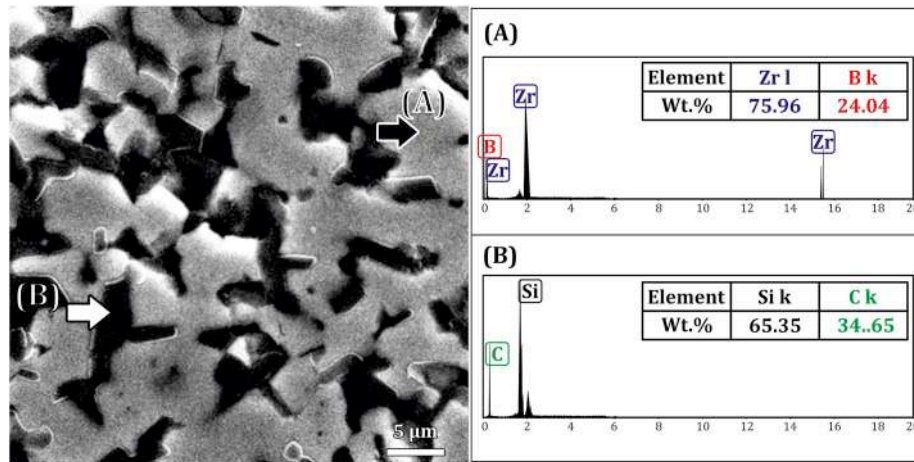


Fig. 1. SEM micrograph and EDS spectra of ZrB<sub>2</sub> and SiC phases in the as-sintered nanocomposite.

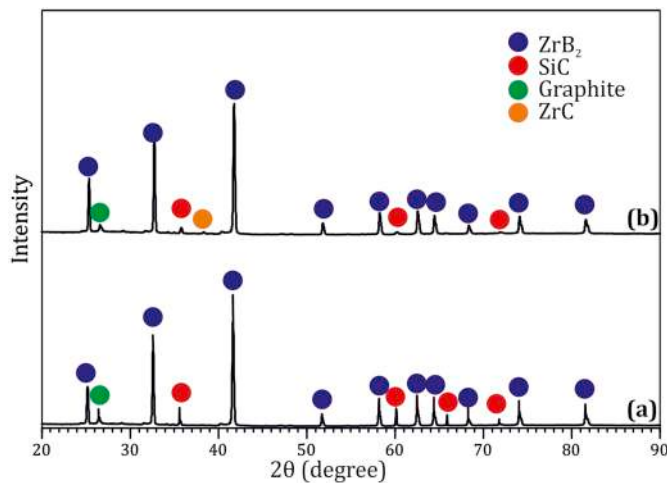


Fig. 2. X-ray diffraction spectra of (a) as-mixed powders and (b) consolidated ZrB<sub>2</sub>-SiC-graphite ceramic.

was used in this research work for characterization of ZrB<sub>2</sub>-SiC-graphite composite sintered by spark plasma at 1800 °C temperature under 35 MPa pressure for 8 min dwell time.

2. Processing and characterizations

Available powders of zirconium diboride (particle size <2 μm, purity >99.8%) and silicon carbide (particle size <3 μm, purity >99.2%) as well as nano-flakes of graphite (thickness <100 nm, purity >99.5%) were purchased as raw materials from Chinese Xuzhou Hongwu company. The weights of starting materials were controlled to provide a mixture of ZrB<sub>2</sub> as the matrix codoped with 25 vol% SiC and 5 wt% graphite. Wet mixing process was performed for 80 min in ethanol medium inside an ultrasonic bath. The composite mixture of ZrB<sub>2</sub>-SiC-graphite was dried on a hot plate magnet and fully dehumidified in an oven. After loading the composite mixture in a graphite die, covered with BN and graphite foil, the sintering was completed in a vacuum spark plasma sintering (SPS) chamber (Nanozint 10i, Khala Poushan Felez Co., Iran) at 1800 °C for 8 min under 35 MPa pressure. After removing the graphite foils from the surface of sintered specimen by grinding, a pellet (thickness: 6 mm, diameter: 2.4 mm) was available for characterization. The graphite foil removal was initially performed via diamond grinding disk. After graphite removal and surface lapping, the sample was ground to 1-μm finish using diamond sand papers. An X-ray

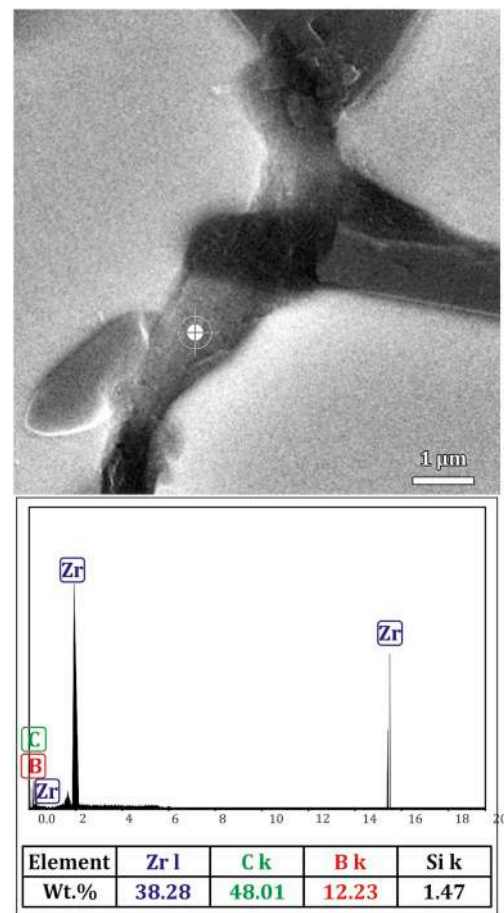


Fig. 3. SEM image and EDS spectrum of an in-situ formed ZrC phase at the interface of ZrB<sub>2</sub> and graphite.

diffractometer (Bruker D8 Advance) was used for phase identification of the sintered sample. Microstructural characterization was carried out employing a field emission scanning electron microscope (Zeiss Ultra Plus) equipped with an energy dispersive spectroscope (Quantax 80) for chemical analysis. Nanostructural investigation was performed using a transmission electron microscope (Philips Tecnai F20) on the prepared sample by the focused ion beam (Gatan 601) method.

Instrumented nano-indentation (Agilent G200, USA) was used to measure the mechanical properties of the achieved composite. Nano-

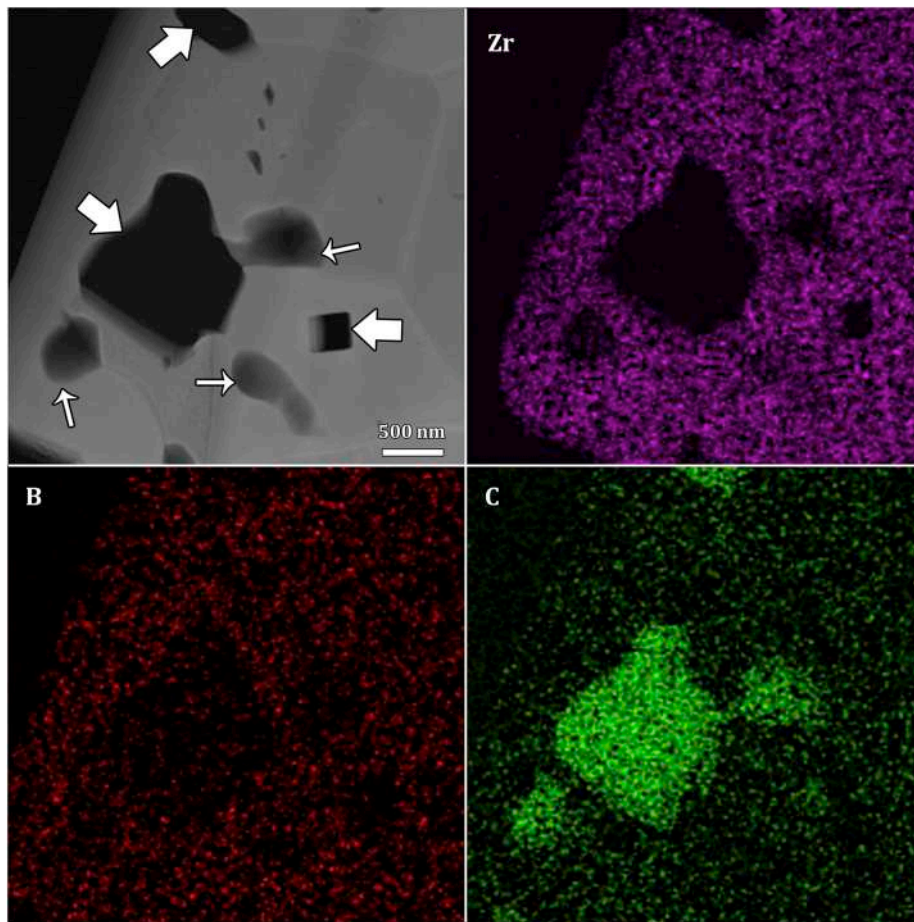


Fig. 4. STEM micrograph and EDS elemental maps of  $ZrB_2$ -SiC-graphite ceramic showing the distribution of Zr, C and B elements.

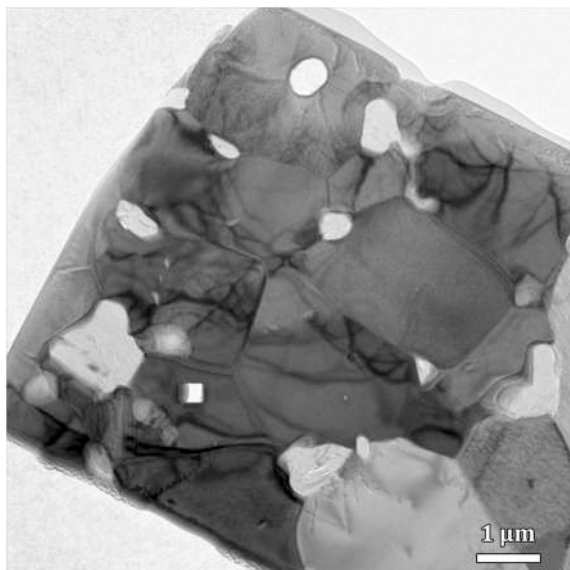


Fig. 5. TEM image of  $ZrB_2$ -SiC-graphite ceramic prepared by the focused ion beam (FIB).

indentation tests were carried out at 25 °C using a Berkovich indenter at maximum load of 400 mN. The loading process prolonged 10 s and then the indenter was hold at the maximum load for extra 5 s. More details about nano-indentation test can be found elsewhere [32].

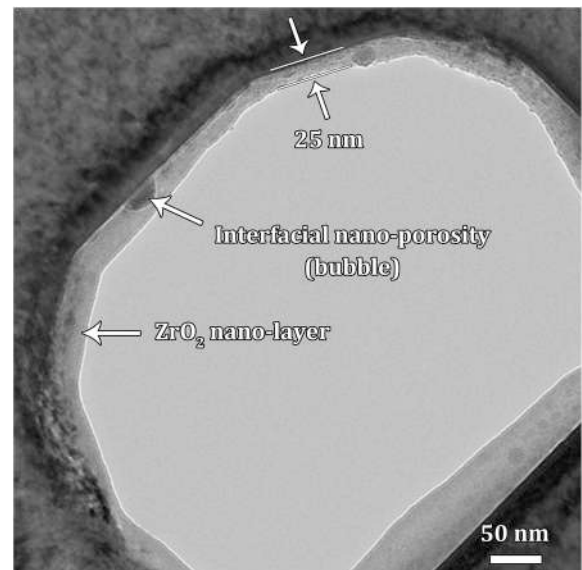


Fig. 6. TEM nanograph of a submicron porosity in the  $ZrB_2$  matrix showing the presence of a nano-sized circumferential amorphous  $ZrO_2$  layer around the pore.

Corresponding load-displacement curves were then analyzed based of Oliver-Pharr (O&P) method [33] to calculate the hardness and elastic modulus of the composite components. The curves were also used to monitor the indentation response of each phase. For each distinct phase

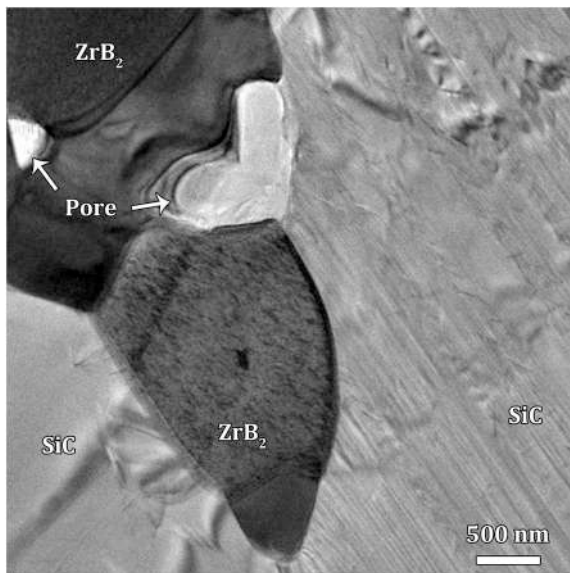


Fig. 7. TEM micrograph showing the interfaces of  $ZrB_2$  and SiC grains and remaining of few submicron pores in the sintered ceramic composite.

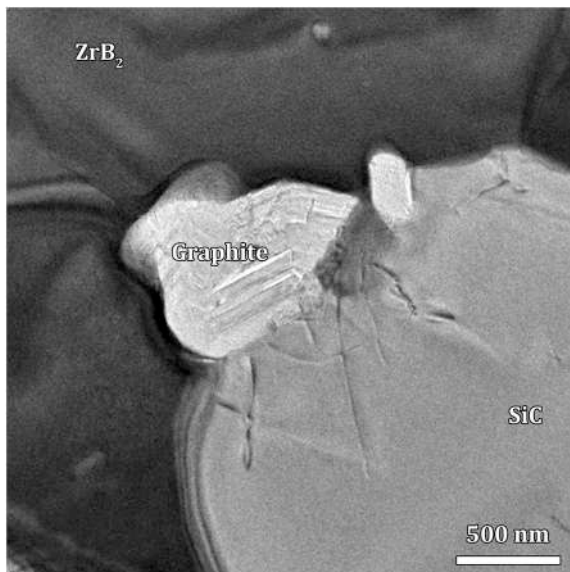


Fig. 8. TEM image showing a submicron graphite between the  $ZrB_2$  and SiC grains.

in the optical microstructure of the composite, at least 10 indents were applied and the average mechanical properties were calculated.

### 3. Results and discussion

Fig. 1 presents the SEM micrograph of the polished surface of as-sintered  $ZrB_2$ -SiC-graphite nanocomposite. No obvious pore is observed in this image which can address the complete densification during the SPS process. The light-colored grains, as the major phase in this figure, belong to the  $ZrB_2$  matrix. The dark-colored phases with distinct boundaries are SiC grains but those with pallid interfaces are graphite nano-flakes, which have been picked up during the polishing due to their intrinsic softness, or may be carbon-induced new phases. A phase analysis by XRD can be helpful for characterization of such in-situ formed phases. In addition, elemental analysis by EDS can also assist the identification process of different phases. In this regard, EDS analyses

were carried out on two distinct points through the light and dark phases shown in Fig. 1. As it can be seen, only the peaks of zirconium and boron were detected for the light phase (marked by black arrow in Fig. 1) that is corresponded to the matrix of  $ZrB_2$ . EDS pattern demonstrates that only the peaks of silicon and carbon were identifies in the dark phase (marked by white arrow in Fig. 1) which can be nominated as SiC additive.

X-ray diffraction patterns of the as-mixed powders/flakes of the starting materials and the as-sintered  $ZrB_2$ -SiC-graphite composite are presented in Fig. 2. As it can be seen in Fig. 2a, the diffraction peaks of all the employed raw materials are detectable in the spectrum of as-processed powder mixture. Only one peak of graphite was identified by XRD test due to its low content as the dopant. Fig. 2b shows the X-ray diffraction pattern of as-consolidated  $ZrB_2$ -SiC-graphite composite. At the investigated range of  $20^\circ < 2\theta < 90^\circ$ , most of the detected peaks belong to crystalline  $ZrB_2$ , however, some peaks of SiC as well as one peak of graphite and one peak of ZrC were also identified. Detection of trace amounts of graphite together with the in-situ formed ZrC phase promotes the hypothesis of partial reaction between graphite and the surface impurity of  $ZrO_2$ . However, some graphite nano-flakes were remained unreacted in the as-sintered composite. In-situ formation of new carbides due to chemical reaction of carbon dopants with the surface oxides of non-oxide ceramics, was previously reported in many research and review papers [7,9–11,34,35]. However, it has been reported that graphene shows non-reactive behavior during the SPS of  $ZrB_2$ -SiC-based composites [13]. It seems that the intensity of graphite peak in the sintered composite (Fig. 2b) is somehow lower than that in the powder mixture (Fig. 2a), may be as a result of its consumption during the synthesis of the ZrC phase.

A high-magnification SEM micrograph of the as-sintered nanocomposite is shown in Fig. 3a. An EDS analysis was captured from the gray-colored phase, indicated by a square, which seems to be different from the main  $ZrB_2$  and SiC grains. The result of chemical analysis is presented in Fig. 3b which verifies the high concentrations of carbon and zirconium elements in such area. Hence, it can be nominated as the in-situ formed ZrC phase which is previously detected through XRD analysis. The location of such new formed phase is microstructurally logical, because it can be supposed that the graphite flakes, located between two  $ZrB_2$  particles, are potentially capable to participate in chemical reactions with the surface oxides of the matrix and convert to the ZrC.

The presence of carbonaceous dopant in the form elemental graphite and/or new formed ZrC compound after sintering process, can be well-clarified through STEM investigation. Therefore, the STEM images of  $ZrB_2$ -SiC-graphite nanocomposite as well as the EDS elemental maps of zirconium, boron and carbon are shown in Fig. 4. Based on these outcomes, the darkest grains (marked by arrows) can be related to the remained graphite flakes and the relatively pallid areas may be attributed to the in-situ formed ZrC phases. The distribution maps of zirconium and boron verify the light-gray-colored background as the  $ZrB_2$  matrix.

Fig. 5 shows an TEM image of  $ZrB_2$ -SiC-graphite composite which has been prepared by the focused ion beam for micro/nanostructural studies. It seems that the sintering of this composite is well-progressed because the grains have fittingly joined together (distinct grain boundaries). Not only there is no large-sized porosity in the sintered structure, but also no evidence of grain coarsening during the consolidation process can be found. Such an excellent sinterability in this UHTC composite can be attributed to both constructive effects of nano-graphite addition and employing the SPS as a modern densification route, as SPS mainly deals with evaporation and consolidation of the sintering material, rather than diffusion phenomenon (grain growth promotion).

As it can be obviously seen in Fig. 5 and addressed before, the excellent connections between the grains which are manifested as clear interfaces during the SPS process, can be attributed to the performance of high-temperature spark plasma. In other words, most of the surface oxide impurities (e.g.  $SiO_2$ ,  $B_2O_3$  and  $ZrO_2$ ) may be removed quickly by

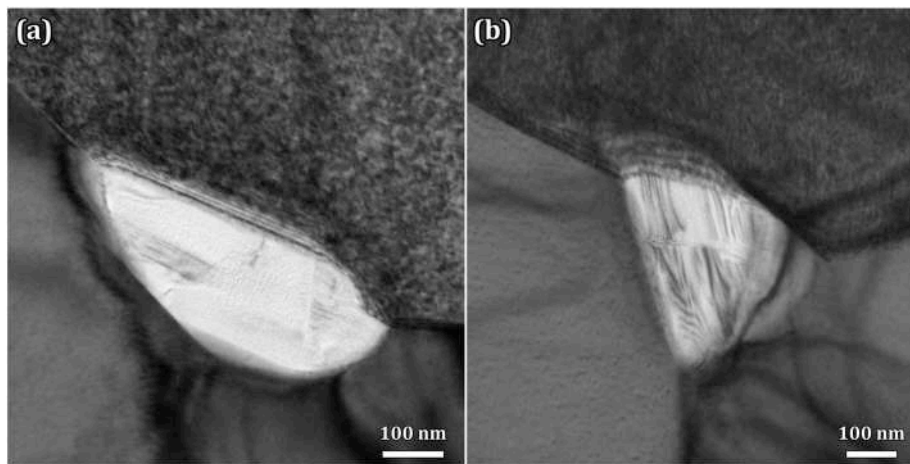


Fig. 9. (a) TEM nanographs showing the graphite nano-flakes between the (a) two and (b) three  $ZrB_2$  grains.

such a phenomenon. Anyway, it seems that few porosities have been remained in the final structure of as-sintered sample, especially in the areas where are not grafted to the graphite nano-flakes as carbon source. For example, an ultrafine porosity is seen in the TEM nanograph of  $ZrB_2$ -SiC-graphite composite (Fig. 6). Such a submicron pore in the  $ZrB_2$  matrix is covered by an amorphous  $ZrO_2$  nano-layer. It is comprehensively reported that the presence of such oxide impurities hinders the sample to be fully densified.

The presence of few submicron pores, e.g. at the interface of  $ZrB_2$  and SiC phases, is also observed in the TEM image of Fig. 7. Regarding to their location (mainly in triple junctions) and irregular morphology, such remained ultrafine porosities in the sintered composite are generally attributed to the harmful oxide impurities. Herein, similar to the negative role of  $ZrO_2$  on densification progress of  $ZrB_2$  ceramics, it seems that the  $SiO_2$  as the oxide film on the surface of SiC grain may also prevented the pores to be completely removed.

Anyway, in comparison with pores marked in Fig. 7, the morphology of interfacial nano-pores (bubble-like) indicated by arrows in Fig. 6, invigorates the hypothesis suggesting simultaneous occurrence of liquid-phase and reactive sintering mechanisms. In other words, whereas graphite additive reductively reacts with surface  $ZrO_2$  and forms ZrC, CO and/or  $CO_2$  may be released as byproducts. Such gases although mainly escaped due to high vacuum of the SPS chamber, but can form nano-bubbles entrapped in the  $SiO_2/B_2O_3$  interfacial liquid phase surrounds  $ZrO_2$  surface nano-layers.

The positive role of nano-graphite addition as a sintering aid for the densification evolution of spark plasma densified  $ZrB_2$ -SiC ceramic is excellently presented in Fig. 8. The microstructure of sintered specimen is free of porosity as a result of graphite presence in that area. Ultrafine graphite nano-flakes, with submicron diameters, have been located at the  $ZrB_2$ /SiC interface. Such graphite nano-flakes and/or probable in-situ formed ZrC phases around them have good connections with both  $ZrB_2$  and SiC grains. Such an impurity cleaning role of carbon additives which assists the porosity elimination, results in enhanced densification and sinterability in the non-oxide ceramics.

Fig. 9 shows the TEM nanographs of  $ZrB_2$ -SiC-graphite nano-composite showing the graphite nano-flakes between the  $ZrB_2$  grains. The laminar morphology of graphite phases, like the graphene nanoplatelets, is clearly seen in these figures. Such graphite nano-flakes not only joined excellently to the grains of  $ZrB_2$  matrix, but also assisted the  $ZrB_2$  particles to completely sinter together. It is observable that the clean boundaries were formed between the grains of matrix phase as a result of oxide elimination by carbon additive. Moreover, the in-situ formation of secondary phases seems to enhance the sinterability via supplying a better condition for the grains to be joined together.

Load-displacement curves of  $ZrB_2$  and SiC phases obtained from

instrumented nano-indentation are representatively shown in Fig. 10. Comparison the indentation response of the phases, nano-indentations were independently applied on  $ZrB_2$  grains, SiC grains and  $ZrB_2$ /SiC interface. The average hardness and Young's modulus of each phase are also presented in Table 1.

As it can be clearly seen in Fig. 10a, besides the smooth load-displacement curves (1, 2 and 4), a pop-in is observed in curve 3. Such a load-displacement curve belongs to the lowest measured hardness (10 GPa) and Young's modulus (257 GPa) of  $ZrB_2$  phase. The pop-in phenomenon in nanoindentation response of zirconium diboride is previously well-described by several brilliant published research works [36–39], and can be attributed to dislocation movement and/or nucleation, when the grain is randomly oriented in situation that provides minimum angle ( $\theta = 0$ ) between applied tension and principle axis of  $ZrB_2$  hexagonal monocrystal. In other word, the basal plane (perpendicular to the principle axis) encounters the maximum applied load, which promotes dislocation movement/nucleation on this plane. Therefore, nevertheless its fully-brittle nature,  $ZrB_2$  seems to show semi-plastic behavior in nano-scale, particularly when the indentation stress applied on the basal planes. Such a nano-scale plastic behavior of zirconium diboride has previously reported as an interfacial densification mechanism during the hot pressing of  $ZrB_2$ -based composites [40]. The obtained mechanical properties of  $ZrB_2$  phase (see Table 1) are also well-adjusted with literatures [37–39], although may be somehow different with other  $ZrB_2$ -based composites [41].

According to Fig. 10b, besides the calculated hardness and Young's modulus of SiC phase which are in good adjustment with the literatures [42,43], pop-ins observed (marked in Fig. 10b) in both curves 1 (lowest measured hardness) and 4 (highest measured hardness). Anyway, whereas curve 1 deals with just one pop-in at about 225 mN load, two distinct pop-ins can be observed in curve 4 at load of 125 and 275 mN, respectively. Such a phenomenon is well-described by Matsumoto et al. [43] and the pop-in occurred in lower load is attributed to the phase transformation and burst of dislocations in SiC single crystals, if the load applied along the basal planes. At higher applied loads, cracking and local failure of the material play the dominant role in pop-in occurrence. Therefore, it can be concluded that the wide range (heterogeneous) distribution of measured hardness and Young's modulus for both  $ZrB_2$  and SiC phases may be due to randomly oriented grains in SPSed composite, which may differently affect the contributing parameters of nano-indentational response, e.g. the angle between basal planes and applied load.

The abovementioned discussions can be confirmed, if the load-displacement curves of the  $ZrB_2$ /SiC interface (Fig. 10c) are taken into account. Although the minimum and average hardness and elastic modulus of the interface show meaningful decrease in comparison with

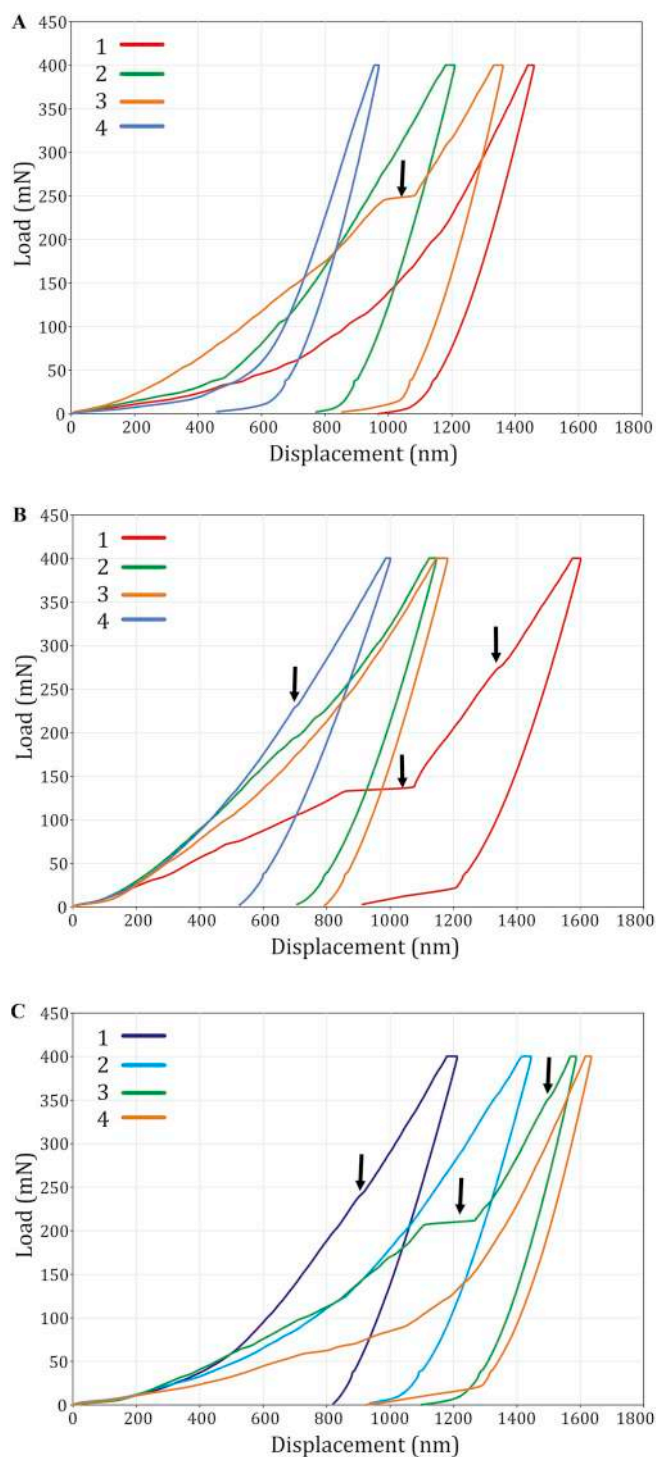


**Fig. 10.** Load-displacement curves obtained from instrumented nano-indentation for 4 representative points of (a)  $ZrB_2$  phase, (b) SiC phase and (c)  $ZrB_2/SiC$  interface in which, curve 1 belongs to indent with maximum, 2 and 3 belong to average and 4 belongs to minimum calculated hardness numbers.

those of  $ZrB_2$  and SiC phases, the shape of load-displacement curves presents both characteristics of the composite's components. The respectively low hardness obtained of applied nano-indenters on the interface, may be due to remained interfacial porosities and/or remained graphite flakes. Similarly, remained porosities and graphite flakes can be considered as the responsible for low interfacial elastic modulus. Anyway, the shape of load-displacement curves somehow resembles the curves of SiC (curve 3 in Fig. 10c) in which, two distinct

**Table 1**

The calculated hardness and Young's modulus of each phase in  $ZrB_2-SiC$ -graphite composite based on O&P method.

Phase	Hardness (GPa)			Young's modulus (GPa)		
	Min	Max	Average	Min	Max	Average
$ZrB_2$	10.0	24.8	15.2	257	576	328
SiC	8.4	29.6	18.3	203	355	306
Interface	7.7	16.4	10.7	233	293	253

(lower and upper) pop-ins can be observed. It seems that SiC plays the dominant role in corresponding indent, which may be attributed to the location of the indenter tip. For instance, if the main part of projected area is located in SiC, the load-displacement curve will tend to that of silicon carbide. Conversely, if the indent projected area is mainly located in  $ZrB_2$  phase, the characteristics of the load-displacement will figure out the curves of zirconium diboride, as can be seen in curves 2 and 4 in Fig. 10c.

Also, the interfacial phases such as remained graphite, zirconium dioxide and possible glassy phases may affect the shape of load-displacement curves at interfaces, based on the volume fraction of the phases and location of indenter tip. SEM/AFM-equipped instrumented nano-indentation test can result in more accurate results, as the location of indent can be precisely determined. The conclusive nano-indentational response of several phases in  $ZrB_2-SiC$ -graphite composite is schematically presented in Fig. 11.

#### 4. Conclusions

$ZrB_2-SiC$ -graphite nanocomposite was fabricated via SPS route at  $1800^\circ C$  for 8 min under 35 MPa. The micro/nanostructure of the sintered ceramic sample was characterized via SEM/STEM/TEM facilities to determine the influence of nano-graphite dopant on the densification and sinterability of UHTC specimen. XRD and EDS analyses were also employed to verify the in-situ formation of secondary phases (such as ZrC) at the interface of graphite and main grains. Although few submicron porosities were identified via nanostructural investigations, the fabrication of a near fully-dense  $ZrB_2$ -based composite was possible by the addition of nano-graphite. Reported observations were related to the positive role of graphite on elimination of surface oxide impurities. Although the measured properties were widely distributed the mechanical properties (hardness and elastic modulus) of the composite showed appropriate adjustment with the previous reports. The hardness of  $ZrB_2$  matrix was measured between the minimum of 10.0 and maximum of 24.8 GPa, whereas 8.4 and 29.6 GPa were calculated as minimum and maximum hardness for SiC reinforcement. Due discussions and illustrations were dedicated to the nano-indentational characteristics of the composite, particularly appeared pop-ins in load-displacement curves.

#### References

- [1] Shahedi Asl M, Ghassemi Kakroudi M. A processing-microstructure correlation in  $ZrB_2-SiC$  composites hot-pressed under a load of 10 MPa. *Univers. J. Mater. Sci.* 2015;3:14–21. <https://doi.org/10.13189/ujms.2015.030103>.
- [2] Shahedi Asl M, Ghassemi Kakroudi M. Fractographical assessment of densification mechanisms in hot pressed  $ZrB_2-SiC$  composites. *Ceram Int* 2014;40:15273–81. <https://doi.org/10.1016/j.ceramint.2014.07.023>.
- [3] Shahedi Asl M, Ghassemi Kakroudi M, Noori S. Hardness and toughness of hot pressed  $ZrB_2-SiC$  composites consolidated under relatively low pressure. *J Alloy Comp* 2015;619:481–7. <https://doi.org/10.1016/j.jallcom.2014.09.006>.
- [4] Shahedi Asl M, Ghassemi Kakroudi M, Golestani-Fard F, Nasiri H. A Taguchi approach to the influence of hot pressing parameters and SiC content on the sinterability of  $ZrB_2$ -based composites. *Int J Refract Metals Hard Mater* 2015;51: 81–90. <https://doi.org/10.1016/j.ijrmhm.2015.03.002>.
- [5] Jaber Zamharir M, Shahedi Asl M, Pourmohammadi Vafa N, Ghassemi Kakroudi M. Significance of hot pressing parameters and reinforcement size on densification behavior of  $ZrB_2-25vol\%$  SiC UHTCs. *Ceram Int* 2015;41:6439–47. <https://doi.org/10.1016/j.ceramint.2015.01.082>.

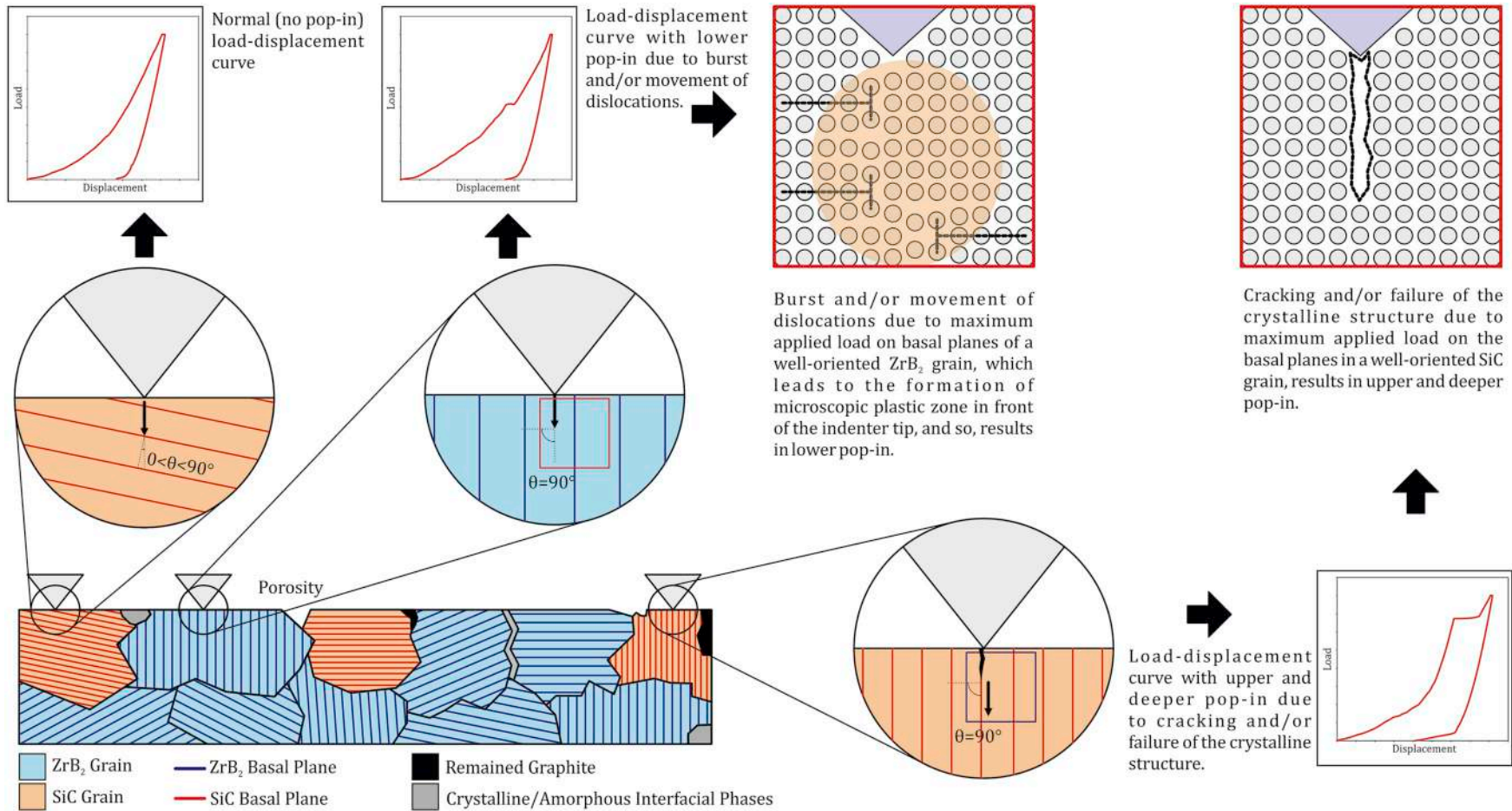


Fig. 11. Schematic view of different nano-indentational response of constituent phases in  $ZrB_2$ -SiC-graphite composites.

- [6] Jaber Zamharir M, Shahedi Asl M, Ghassemi Kakroudi M, Pourmohammadi Vafa N, Jaber Zamharir M. Significance of hot pressing parameters and reinforcement size on sinterability and mechanical properties of ZrB<sub>2</sub>-25vol% SiC UHTCs. *Ceram Int* 2015;41:9628–36. <https://doi.org/10.1016/j.ceramint.2015.04.027>.
- [7] Shahedi Asl M, Nayebi B, Ahmadi Z, Jaber Zamharir M, Shokouhimehr M. Effects of carbon additives on the properties of ZrB<sub>2</sub>-based composites: a review. *Ceram Int* 2018;44:7334–48. <https://doi.org/10.1016/j.ceramint.2018.01.214>.
- [8] Azizian-Kalanderaragh Y, Namini AS, Ahmadi Z, Shahedi Asl M. Reinforcing effects of SiC whiskers and carbon nanoparticles in spark plasma sintered ZrB<sub>2</sub> matrix composites. *Ceram Int* 2018;44:19932–8. <https://doi.org/10.1016/j.ceramint.2018.07.258>.
- [9] Farahbakhsh I, Ahmadi Z, Shahedi Asl M. Densification, microstructure and mechanical properties of hot pressed ZrB<sub>2</sub>-SiC ceramic doped with nano-sized carbon black. *Ceram Int* 2017;43:8411–7. <https://doi.org/10.1016/j.ceramint.2017.03.188>.
- [10] Shahedi Asl M, Golmohammadi F, Ghassemi Kakroudi M, Shokouhimehr M. Synergetic effects of SiC and Csf in ZrB<sub>2</sub>-based ceramic composites. Part I: densification behavior. *Ceram Int* 2016;42:4498–506. <https://doi.org/10.1016/j.ceramint.2015.11.139>.
- [11] Shahedi Asl M, Kakroudi MG, Farahbakhsh I, Mazinani B, Balak Z. Synergetic effects of SiC and Csf in ZrB<sub>2</sub>-based ceramic composites. Part II: grain growth. *Ceram Int* 2016;42:18612–9. <https://doi.org/10.1016/j.ceramint.2016.08.205>.
- [12] Shahedi Asl M, Farahbakhsh I, Nayebi B. Characteristics of multi-walled carbon nanotube toughened ZrB<sub>2</sub>-SiC ceramic composite prepared by hot pressing. *Ceram Int* 2016;42:1950–8. <https://doi.org/10.1016/j.ceramint.2015.09.165>.
- [13] Shahedi Asl M, Nayebi B, Shokouhimehr M. TEM characterization of spark plasma sintered ZrB<sub>2</sub>-SiC-graphene nanocomposite. *Ceram Int* 2018;44:15269–73. <https://doi.org/10.1016/j.ceramint.2018.05.170>.
- [14] Shahedi Asl M, Ghassemi Kakroudi M. Characterization of hot-pressed graphene reinforced ZrB<sub>2</sub>-SiC composite. *Mater Sci Eng A* 2015;625:385–92. <https://doi.org/10.1016/j.msea.2014.12.028>.
- [15] Shahedi Asl M, Zamharir MJ, Ahmadi Z, Parvizi S. Effects of nano-graphite content on the characteristics of spark plasma sintered ZrB<sub>2</sub>-SiC composites. *Mater Sci Eng A* 2018;716:99–106. <https://doi.org/10.1016/j.msea.2018.01.038>.
- [16] Parvizi S, Ahmadi Z, Zamharir MJ, Shahedi Asl M. Synergistic effects of graphite nano-flakes and submicron SiC particles on the characteristics of spark plasma sintered ZrB<sub>2</sub> nanocomposites. *Int J Refract Metals Hard Mater* 2018;75:10–7. <https://doi.org/10.1016/j.ijrmhm.2018.03.017>.
- [17] Feng Y, Guo Y, Ling Z, Zhang X. Investigation on machining performance of micro-holes EDM in ZrB<sub>2</sub>-SiC ceramics using a magnetic suspension spindle system. *Int J Adv Manuf Technol* 2019;101:2083–95. <https://doi.org/10.1007/s00170-018-1316-1>.
- [18] Li H, Wang Z, Wang Y, Liu H, Bai Y. Micro-EDM drilling of ZrB<sub>2</sub>-SiC-graphite composite using micro sheet-cylinder tool electrode. *Int J Adv Manuf Technol* 2017;92:2033–41. <https://doi.org/10.1007/s00170-017-0296-z>.
- [19] Cheng Y, Qi Y, Hu P, Zhou S, Chen G, An J, Jin K, Han W. ZrB<sub>2</sub>-SiC-G composite prepared by spark plasma sintering of in-situ synthesized ZrB<sub>2</sub>-SiC-C composite powders. *J Am Ceram Soc* 2016;99:2131–7. <https://doi.org/10.1111/jace.14192>.
- [20] Babapoor A, Asl MS, Ahmadi Z, Namini AS. Effects of spark plasma sintering temperature on densification, hardness and thermal conductivity of titanium carbide. *Ceram Int* 2018;44:14541–6. <https://doi.org/10.1016/j.ceramint.2018.05.071>.
- [21] Sabahi Namini A, Ahmadi Z, Babapoor A, Shokouhimehr M, Shahedi Asl M. Microstructure and thermomechanical characteristics of spark plasma sintered TiC ceramics doped with nano-sized WC. *Ceram Int* 2019;45:2153–60. <https://doi.org/10.1016/j.ceramint.2018.10.125>.
- [22] Sabahi Namini A, Azadbeh M, Shahedi Asl M. Effect of TiB<sub>2</sub> content on the characteristics of spark plasma sintered Ti-TiB<sub>2</sub> w composites. *Adv Powder Technol* 2017;28:1564–72. <https://doi.org/10.1016/j.apt.2017.03.028>.
- [23] Shahedi Asl M, Sabahi Namini A, Motallebzadeh A, Azadbeh M. Effects of sintering temperature on microstructure and mechanical properties of spark plasma sintered titanium. *Mater Chem Phys* 2018;203:266–73. <https://doi.org/10.1016/j.matchemphys.2017.09.069>.
- [24] Sabahi Namini A, Azadbeh M, Shahedi Asl M. Effects of in-situ formed TiB whiskers on microstructure and mechanical properties of spark plasma sintered Ti-B<sub>4</sub>C and Ti-TiB<sub>2</sub> composites. *Sci Iran* 2018;25:762–71. <https://doi.org/10.24200/sci.2017.4499>.
- [25] Kitiwan M, Ito A, Goto T. Spark plasma sintering of TiN-TiB<sub>2</sub>-hBN composites and their properties. *Ceram Int* 2015;41:4498–503. <https://doi.org/10.1016/j.ceramint.2014.11.144>.
- [26] Shayesteh F, Delbari SA, Ahmadi Z, Shokouhimehr M, Shahedi Asl M. Influence of TiN dopant on microstructure of TiB<sub>2</sub> ceramic sintered by spark plasma. *Ceram Int* 2018. <https://doi.org/10.1016/j.ceramint.2018.11.228>.
- [27] Shahedi Asl M, Ahmadi Z, Parvizi S, Balak Z, Farahbakhsh I. Contribution of SiC particle size and spark plasma sintering conditions on grain growth and hardness of TiB<sub>2</sub> composites. *Ceram Int* 2017;43:13924–31. <https://doi.org/10.1016/j.ceramint.2017.07.121>.
- [28] Ahmadi Z, Nayebi B, Shahedi Asl M, Farahbakhsh I, Balak Z. Densification improvement of spark plasma sintered TiB<sub>2</sub>-based composites with micron-, submicron- and nano-sized SiC particulates. *Ceram Int* 2018;44:11431–7. <https://doi.org/10.1016/j.ceramint.2018.03.202>.
- [29] Dashti Germi M, Hamidzadeh Mahaseni Z, Ahmadi Z, Shahedi Asl M. Phase evolution during spark plasma sintering of novel Si<sub>3</sub>N<sub>4</sub>-doped TiB<sub>2</sub>-SiC composite. *Mater Char* 2018;145:225–32. <https://doi.org/10.1016/j.matchar.2018.08.043>.
- [30] Hamidzadeh Mahaseni Z, Dashti Germi M, Ahmadi Z, Shahedi Asl M. Microstructural investigation of spark plasma sintered TiB<sub>2</sub> ceramics with Si<sub>3</sub>N<sub>4</sub> addition. *Ceram Int* 2018;44:13367–72. <https://doi.org/10.1016/j.ceramint.2018.04.171>.
- [31] Delbari SA, Nayebi B, Ghasali E, Shokouhimehr M, Shahedi Asl M. Spark plasma sintering of TiN ceramics codoped with SiC and CNT. *Ceram Int* 2019;45:3207–16. <https://doi.org/10.1016/j.ceramint.2018.10.223>.
- [32] Nekahi S, Sadegh Moghanlou F, Vajdi M, Ahmadi Z, Motallebzadeh A, Shahedi Asl M. Microstructural, thermal and mechanical characterization of TiB<sub>2</sub>-SiC composites doped with short carbon fibers. *Int J Refract Metals Hard Mater* 2019; 82:129–35. <https://doi.org/10.1016/j.ijrmhm.2019.04.005>.
- [33] Pharr GM, Oliver WC. Measurement of thin film mechanical properties using nanoindentation. *MRS Bull* 1992;17:28–33. <https://doi.org/10.1557/S0883769400041634>.
- [34] Khoeiini M, Nemati A, Zakeri M, Tamizifar M, Samadi H. Comprehensive study on the effect of SiC and carbon additives on the pressureless sintering and microstructural and mechanical characteristics of new ultra-high temperature ZrB<sub>2</sub> ceramics. *Ceram Int* 2015;41:11456–63. <https://doi.org/10.1016/j.ceramint.2015.05.110>.
- [35] Shahedi Asl M. A statistical approach towards processing optimization of ZrB<sub>2</sub>-SiC-graphite nanocomposites. Part I: relative density. *Ceram Int* 2018;44: 6935–9. <https://doi.org/10.1016/j.ceramint.2018.01.122>.
- [36] Guicciardi S, Melandri C, Monteverde FT. Characterization of pop-in phenomena and indentation modulus in a polycrystalline ZrB<sub>2</sub> ceramic. *J Eur Ceram Soc* 2010; 30:1027–34. <https://doi.org/10.1016/j.jeurceramsoc.2009.10.014>.
- [37] Csanádi T, Grasso S, Kovalčíková A, Dusza J, Reece M. Nanohardness and elastic anisotropy of ZrB<sub>2</sub> crystals. *J Eur Ceram Soc* 2016;36:239–42. <https://doi.org/10.1016/j.jeurceramsoc.2015.09.012>.
- [38] Csanádi T, Kovalčíková A, Dusza J, Fahrnholtz WG, Hilmas GE. Slip activation controlled nanohardness anisotropy of ZrB<sub>2</sub> ceramic grains. *Acta Mater* 2017;140: 452–64. <https://doi.org/10.1016/j.actamat.2017.08.061>.
- [39] Csanádi T, Naughton-Duszová A, Dusza J. Anisotropic slip activation via homogeneous dislocation nucleation in ZrB<sub>2</sub> ceramic grains during nanoindentation. *Scripta Mater* 2018;152:89–93. <https://doi.org/10.1016/j.scriptamat.2018.04.025>.
- [40] Nayebi B, Shahedi Asl M, Ghassemi Kakroudi M, Farahbakhsh I, Shokouhimehr M. Interfacial phenomena and formation of nano-particles in porous ZrB<sub>2</sub>-40 vol% B<sub>4</sub>C UHTC. *Ceram Int* 2016;42:17009–15. <https://doi.org/10.1016/j.ceramint.2016.07.208>.
- [41] Cheng EJ, Li Y, Sakamoto J, Han S, Sun H, Noble J, Katsui H, Goto T. Mechanical properties of individual phases of ZrB<sub>2</sub>-ZrC eutectic composite measured by nanoindentation. *J Eur Ceram Soc* 2017;37:4223–7. <https://doi.org/10.1016/j.jeurceramsoc.2017.05.031>.
- [42] Guicciardi S, Balbo A, Sciti D, Melandri C, Pezzotti G. Nanoindentation characterization of SiC-based ceramics. *J Eur Ceram Soc* 2007;27:1399–404. <https://doi.org/10.1016/j.jeurceramsoc.2006.05.057>.
- [43] Matsumoto M, Huang H, Harada H, Kakimoto K, Yan J. On the phase transformation of single-crystal 4H-SiC during nanoindentation. *J Phys D Appl Phys* 2017;50:265303. <https://doi.org/10.1088/1361-6463/aa7489>.